DOI:10.13476/j.cnki.nsbdqk.2021.0053
LI X Y,ZHAO Q,YAO T,et al. The change and prediction of temperature and precipitation in the Dawen River basin using the statistical downscaling model (SDSM)[J]. South-to-North Water Transfers and Water Science & Technology,2021,19(3):496-510. (in Chinese)

The change and prediction of temperature and precipitation in the Dawen River basin using the statistical downscaling model (SDSM)

LI Xinying,ZHAO Qiang,YAO Tian,SHEN Zhentao,RAN Pengyu

(School of Water Conservancy and Environment,University of Jinan,Jinan 250022,China)

Abstract:In order to explore the climate change in the Dawen River basin,based on the data of six weather stations in the Dawen River basin from 1966 to 2017,Mann-Kendall test and wavelet analysis were used to study the temperature and precipitation trends,mutations and cycles in the region. In addition,based on the three scenarios of RCP2.6,RCP4.5,and RCP8.5 under the CanESM2 model,SDSM was used to compare and analyze the future climate change of the Dawen River basin. The results revealed that:the annual mean temperature of the Dawen River basin had increased significantly since 1966 ($p<0.01$);in different scenarios,the spatial distribution of the projected maximum temperature,minimum temperature and precipitation will hardly change compared with that in history;the temperature and precipitation in the Dawen River basin will generally increase in the future. The rising trend of maximum and minimum temperature under the three scenarios is in the EP<MP<LP,and June and November was the months with the highest increase;the future precipitation will have the highest increase in July and August. Under the RCP4.5 and RCP8.5 scenarios,the annual maximum and minimum temperatures in the future will increase with the increase in time scale.

Key words:Dawen River basin;Mann-Kendall test;wavelet analysis;SDSM;climate prediction

Chinese Library Classification No.:P333;TV213 **Document Code**:A OSID:

1 Introduction

Global climate change is currently one of the hot topics of concern for academics,governments,and individuals[1-3]. According to the Intergovernmental Panel on Climate Change (IPCC),the current global warming had exceeded the pre-industrial level by 1.5 ℃[4]. Over the years,global temperatures have continued to warm,extreme weather events had occurred frequently,and natural disasters had proliferated. On December 26,2004,for example,an earthquake occurred on the Indonesian island of Sumatra,generating a large-scale tsunami;on August 29,2005,Hurricane Katrina made

Received:2020-11-03 **Revised**:2021-04-07 **Online publishing**:2021-04-23
Online publishing address:https://kns.cnki.net/kcms/detail/13.1430.TV.20210423.1025.006.html
Fund:National Natural Science Foundation of China (41471160)
Author's brief:LI Xinying (1997-),male,Tengzhou Shandong,mainly engaged in hydrology and water resources and climate change. E-mail:1030822250@qq.com
Corresponding author:ZHAO Qiang (1977-),male,Tai'an Shandong,professor,doctor,mainly engaged in water cycle and efficient use of water resources,climate change,Tourism resource evaluation. E-mail:stu_zhaoq@ujn.edu.cn

landfall in Louisiana and Mississippi, USA; in 2008, the extremely intense tropical cyclone Nargis swept the coastline of southern Myanmar. The occurrence of these natural disasters all caused major losses to the economy and massive loss of life[1-3]. It is estimated that the annual global economic loss due to natural disasters exceeds 50 billion dollars, and the annual loss of life is about 250,000[5]. Among these deaths, more than 60,000 inhabitants of developing countries die from extreme weather events every year[6]. China's climate change problems are even more serious. According to statistical data, from 1951 to 2017, the annual mean surface temperature in China exceeded the global value, with a growth rate of 0.24 ℃/(10 a)[7]. Observations had shown that regional climate change will lead to changes in various natural and biological systems[8]. Events such as the glacial retreat, the permafrost melting, and the extension of the growing season in mid and high latitude areas continued to occur throughout the country. The occurrence of these events will inevitably have an undeniable impact on the environment, ecology, agriculture, water resources, the economy, society, and even human health[9-13].

At present, the global climate model (GCM) is recognized as the main method for studying future climate change, but the direct use of GCMs to predict climate often ignores small-scale issues such as vegetation conditions, which may lead to insufficient accuracy of the output results[14]. The statistical downscaling (SD) method developed a quantitative relationship between two sets of predictors-large-scale atmospheric variables and local surface variables-under the conditions of climate change, and keeps the relationship unchanged[15-16]. Compared with other approaches, this ensured that the SD technique is not computationally intensive and can easily be applied to the outputs of different GCM experiments[15,17]. The SDSM model is a downscaling method based on the windows interface, and it is very interactive and practical. It converts large-scale, low-resolution GCMs output information into regional-scale ground climate change information, which makes up for the limitations of GCMs for regional climate prediction. Not only that, the SDSM model can select any atmospheric circulation data as the input data. In addition, compared with other models, not only the SDSM model improves the regional resolution, but also its calculation method is more and less computationally expensive, which is its biggest advantage.

The Dawen River basin is a typical representative river basin in the central and southern part of Shandong Province in eastern China. Analyzing the climate change in the Dawen River basin from 1966 to 2017 and then projecting the future climate will not only reveal the climate change trend and lay the foundation for the next steps in the Dawen River basin climate change impact and internal cause research, but will also provide guidance for local governments to respond to climate change and direct agricultural production activities. although the results of research on climate change in the basin have been quite fruitful[18-19], the prediction of the future climate of the basin under different scenarios, especially the research on small sub-basins, is still not thorough enough. Based on the daily meteorological data from six weather stations in the Dawen River basin, this study examined the trends, mutations, and periods of temperature and precipitation in this region. In addition, a comparative analysis of the future maximum temperature, minimum temperature, and precipitation changes in the Dawen River basin under the RCP2.6, RCP4.5, and RCP8.5 emission scenarios was conducted.

2 Materials and Methods

2.1 Study area

The Dawen River basin is located between 35°37′30″-36°32′30″N latitude and 116°11′15″-118°0′0″E longitude, in the western part of central Shandong Province. The basin covers a drainage area of approximately 8,634 km^2 and its total length is 209 km. The water system is developed, originating at the northern foot of Xuangu Mountain in Shandong, where it gathers many direct currents from the Huitai Mountain and Meng Mountain branches, and flows from east to west through Laiwu,

Xintai, Tai′an, Feicheng, Ningyang, Wenshang, and Dongping counties and cities. The terrain is high in the north, low in the south, high in the east, and low in the west, with Mount Tai in the north, the Yimeng Mountains in the south, the Lushan Mountains in the east, and Dongping Lake in the west. In terms of climate, the average annual precipitation in the Dawen River basin ranges from 640 to 760 mm, and the annual average temperature varies from 12 to 14 ℃. Spring winds are severe and dry, and temperatures warm quickly; summer is hot and rainy, and precipitation is concentrated; autumn temperatures drop sharply, and precipitation decreases daily; and winter is cold and dry, with little rain and snow, all of which are typical characteristics of a temperate continental monsoon climate.

2.2 Data

Daily temperature and precipitation datasets were acquired from the website of the China Meteorological Data Service Center (http://data.cma.cn/). These are two of the best meteorological datasets available for China and have been subject to strict quality control by both the World Meteorological Organization (WMO) and the China Meteorological Administration (CMA). As a result, these datasets are widely used in research related to climate change[20-21]. For various reasons, however, there are always missing meteorological data. The linear interpolation was used to fill the data gaps during the study period. The missing data at the beginning and end of the time series were replaced by the average values of these months in all other years[22] and stations with >5% missing data or data missing for more than 3 months were eliminated. Based on the above principles, this investigation selected the daily temperature data of three meteorological stations in the Dawen River basin-Taishan Station, Tai′an Station, and Yiyuan Station-for the 52-year period from 1966 to 2017, and strictly controlled the quality of these meteorological data. To more accurately calculate the precipitation in the study area, this investigation also selected the daily precipitation data of three meteorological stations surrounding the basin-Zichuan, Yanzhou, and Chaoyang-for the same 52-year period.

The SDSM primarily requires three types of data: (1) Measured data of the river basin. This study selected the 40-year meteorological data of Mount Tai, Yiyuan, Yanzhou, and Chaoyang in the study area from 1976 to 2015, mainly including daily maximum temperature (T_{max}), minimum temperature (T_{min}), and precipitation data (P). These data were quality controlled using the aforementioned methods. (2) A large-scale reanalysis dataset from the National Center for Environmental Prediction (NCEP) consisting of 2.5°×2.5° latitude and longitude grid data. The grid near the study area was selected in order to cover all meteorological stations. (3) Atmospheric circulation data. Through the verification of Calibration Model in SDSM, under CanEMS2 scenario, the R^2 of maximum and minimum temperature of each station is greater than 0.7, and the R^2 of rainfall is greater than 0.5, which meets the accuracy requirements. Therefore, the CanEMS2 future climate scenario model was selected and the data were used as the main input data of the downscaling model to obtain future weather data in the study area.

2.3 Methods

We first detected the trend features of climate variables based on the time series of the annual precipitation and annual mean temperature datasets from six meteorological stations. The spatial distributions of temperature and precipitation were analyzed using ArcGIS software. On this basis, the future trends of temperature and precipitation in different scenarios were studied.

2.3.1 Linear tendency estimation

Linear regression uses the principle of data statistics to determine the correlation between a hydrometeorological sequence and its corresponding time, which is then utilized to predict future changes in the time series[23-25].

$$Y(t)=at+b \tag{1}$$

where a is the linear trend term, such that $a>0$ indicates that the climate variables increase with time and $a<0$ indicates that the climate variables de-

crease with time. The larger the value of a, the more obvious the change trend.

2.3.2 Mann-Kendall test

The nonparametric Mann-Kendall trend test was used. Given its low sensitivity to abnormal values in time series, it is effective for identifying monotonic trends and mutation points in meteorological time series. For this reason, it is widely used in the trend analysis of climate and hydrological time series[26-28]. Assuming a time series $X=\{x_1, x_2, \cdots, x_{n-1}, x_n\}$ that does not exhibit a constant trend throughout the length of the time series.

$d_k(2\leqslant k\leqslant N)$ is defined as:

$$d_k=\sum_{i=1}^{n-1}\sum_{j=i+1}^{n} r_i \tag{2}$$

$$r_i=\begin{cases}1 & \text{if} \quad x_j>x_j\\ 0 & \text{if} \quad x_j\leqslant x_j\end{cases} \tag{3}$$

The random sequence d_k approximately obeys a normal distribution.

The expected value $E(d_k)$ and variance $\mathrm{Var}(d_k)$ are defined as:

$$E(d_k)=\frac{k(k-1)}{4} \tag{4}$$

$$\mathrm{Var}(d_k)=\frac{k(k-1)(2k+5)}{72} \tag{5}$$

The statistic UF is defined as:

$$\mathrm{UF}(d_k)=\frac{d_k-E(d_k)}{\sqrt{\mathrm{Var}(d_k)}} \tag{6}$$

The above calculation process is then applied to the inverse sequence of X: $X'=\{x_n, x_{n-1}, \cdots, x_1\}$, and the above process is repeated to obtain $\mathrm{UF}'(d_k)$;

$$\mathrm{UB}(d_k)=-\mathrm{UF}'(d_k) \tag{7}$$

From the intersection of the UB and UF curves along with their ranges, we can determine the start and duration of the mutation[29]. $\mathrm{UF}>0$ indicates that the sequence is on the rise; $\mathrm{UF}<0$ indicates that the sequence exhibits a downward trend. If the curve is greater than 1.96 (significance test), this means the upward trend is obvious, otherwise, the upward trend is not obvious.

2.3.3 Wavelet analysis

Wavelet analysis is a mathematical tool that has recently been developed and quickly applied in many fields, such as image processing and speech analysis. It is another major breakthrough following Fourier analysis. The concept of wavelet transform was first proposed by the French engineer Jean Morlet. It is a basic mathematical method used to approximate a signal or function with a cluster of wavelet functions[30]. Since wavelet analysis is particularly advantageous in signal processing, it is widely used in the analysis and research of the time-frequency structure of meteorological and hydrological sequences[31-34].

In wavelet analysis, the basic wavelet function $\Psi(t)$ satisfies certain conditions. It can form a cluster of functions through scale expansion and translation on the time axis:

$$\Psi_{a,b}(t)=|a|^{-1/2}\Psi\left(\frac{t-b}{a}\right) \quad a,b\in R, a\neq 0 \tag{8}$$

where: $\Psi_{a,b}(t)$ is the subwavelet; a is the scale factor, reflecting the period length of the wavelet; and b is the translation factor, reflecting the shift in time.

The continuous wavelet transform $W_f(a,b)$ is defined as:

$$W_f(a,b)=|a|^{-1/2}\int_{-\infty}^{\infty} f(t)\overline{\Psi}\left(\frac{t-b}{a}\right)\mathrm{d}t \tag{9}$$

where $W_f(a,b)$ is a wavelet transform coefficient; $\Psi(t)$ is a given wavelet function; $f(t)$ is a signal or square integrable function; and $\overline{\Psi}\left(\frac{t-b}{a}\right)$ is a complex conjugate function. If $f(t)$ is equal to $\overline{\Psi}_{a,b}(t)$, the wavelet coefficient at this point is taken as 1.

The discrete wavelet transform form of $W_f(a,b)$ is

$$W_f(a,b)=|a|^{-1/2}\Delta t\sum_{k=1}^{N} f(k\Delta t)\overline{\Psi}\left(\frac{k\Delta t-b}{a}\right) \tag{10}$$

In actual research, the most important procedure is to obtain the wavelet coefficients from the wavelet transform equation, and then use these coefficients to analyze the time-frequency change characteristics of the time series.

The square value of the wavelet coefficient is integrated in the b domain to derive the wavelet variance, using the following formula:

$$\mathrm{Var}(a)=\int_{-\infty}^{\infty}|W_f(a,b)|^2\mathrm{d}b \tag{11}$$

The discrete equation is

$$\mathrm{Var}(a)=\frac{1}{n}\sum_{t-1}^{w}W^2(a,x_t) \tag{12}$$

where: $W^2(a, x_t)$ is the scale a, time t square of the wavelet coefficient or the square of the coefficient modulus at x_t, and n is the length of the sequence.

2.3.4 Climate change prediction

This study selected the daily maximum temperature (T_{max}), minimum temperature (T_{min}), and precipitation data (P) from the Mount Tai, Tai'an, Zichuan, Yiyuan, Yanzhou, and Chaoyang meteorological stations, and these data had undergone strict quality control. Then, based on the observation data from the meteorological stations in the study area and the NCEP reanalysis data, the predictors of the meteorological elements were selected. Next, using the designated predicted values and predictor variables, the simulated data were verified by the measured data, and the parameters of the regression equation were calculated according to the least squares method. Ultimately, the weather generator was utilized to verify the calibration model. Based on the RCP2.6, RCP4.5, and RCP8.5 scenario data in the CanESM2 model, the SDSM4.2 model that was constructed was used to simulate the future daily maximum temperature, minimum temperature, and precipitation data in the study area. The specific operation is shown in Fig. 1.

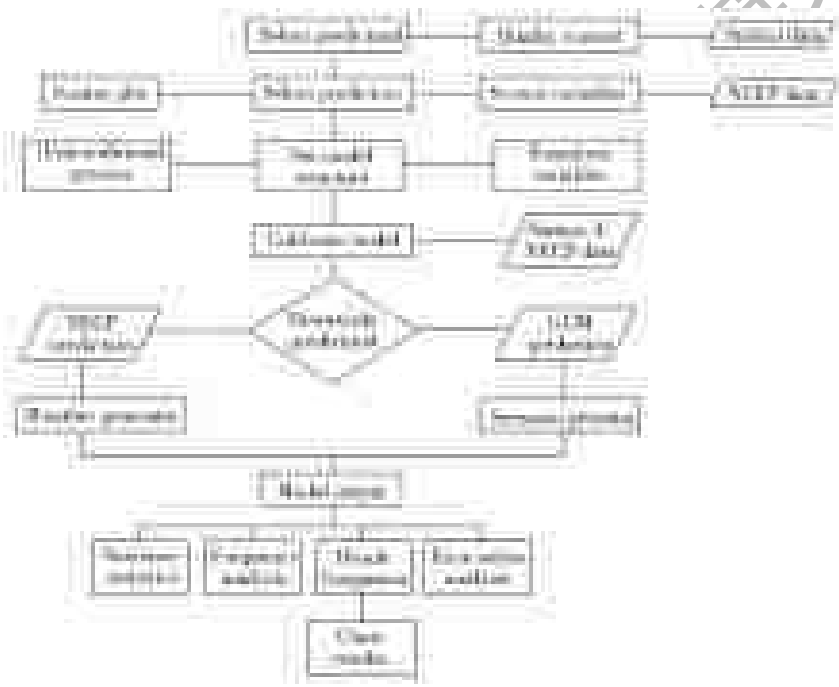

Fig. 1 The flow diagram of SDSM

3 Results

3.1 Analysis of temporal characteristics of climate change

3.1.1 Analysis of temperature characteristics

The linear trend estimation (Fig. 2(a)), the Mann-Kendall test (Fig. 2(b)) and the wavelet analysis(Fig. 2(c))are performed on the 1966-2017 average temperature data from six meteorological stations in the study area.

The results of Fig. 2(a) reveal that the annual mean temperature of the Dawen River basin increased significantly ($p<0.01$) overall from 1966 to 2017, at an average warming rate of approximately 0.32 ℃/(10 a). The Mann-Kendall test graph (Fig. 2(b)) shows that before 1988, the UF statistical value fluctuated around zero, indicating that there is no obvious trend in the annual average temperature from 1966 to 1988. In the 1990s, however, the UF statistics began to gradually increase, indicating that the temperature was rising. The UF and UB curves intersect in 1994 and 1996, and both of these intersection points are within the 95% confidence interval, indicating that the annual average temperature of the study area fluctuated drastically during the five years from 1993 to 1997.

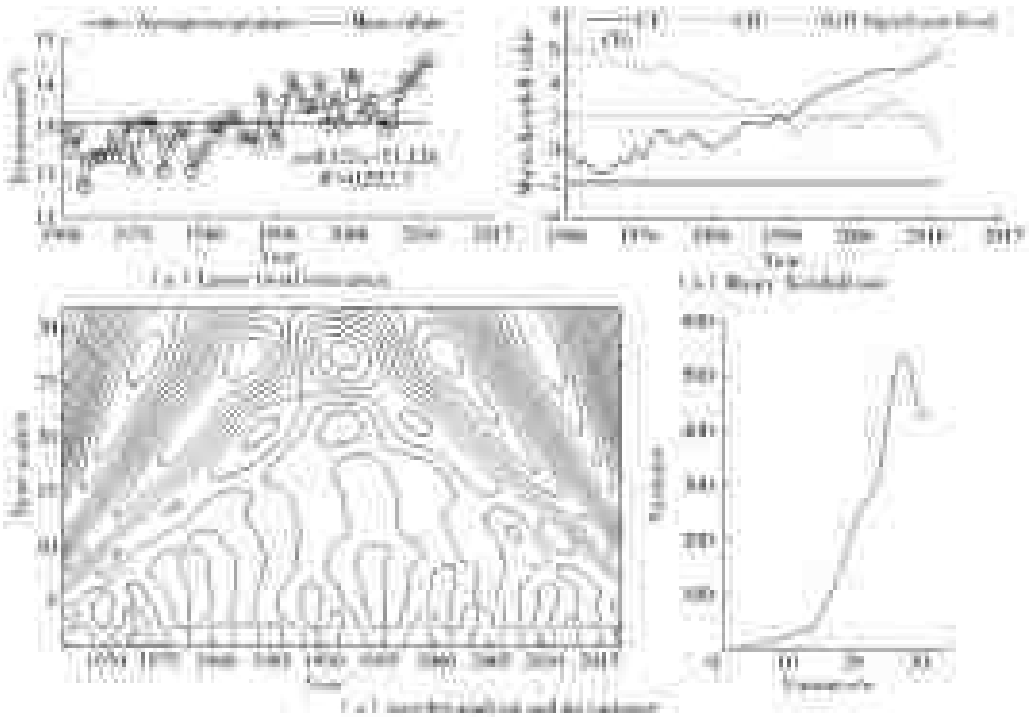

Fig. 2 Time series analysis of annual temperature in the Dawen River basin

The temperature wavelet analysis and variance diagram of the Dawen River basin from 1966 to 2017 is presented in Fig. 2(c). It is obvious that there was a visible temperature alternation, with low temperature areas centered on 1974 and 1992, and high temperature areas centered on 1983 and 2001 in the basin. According to the wavelet variance diagram, the peak value of the wavelet variance was highest when the time scale is 28 years, which is the first main period.

3.1.2 Analysis of precipitation time characteristics

The linear trend estimation (Fig. 3(a)), Mann-Kendall test (Fig. 3(b)) and wavelet analysis (Fig. 3(c)) are performed on the 1966-2017 average precipitation data of six meteorological stations in the study area.

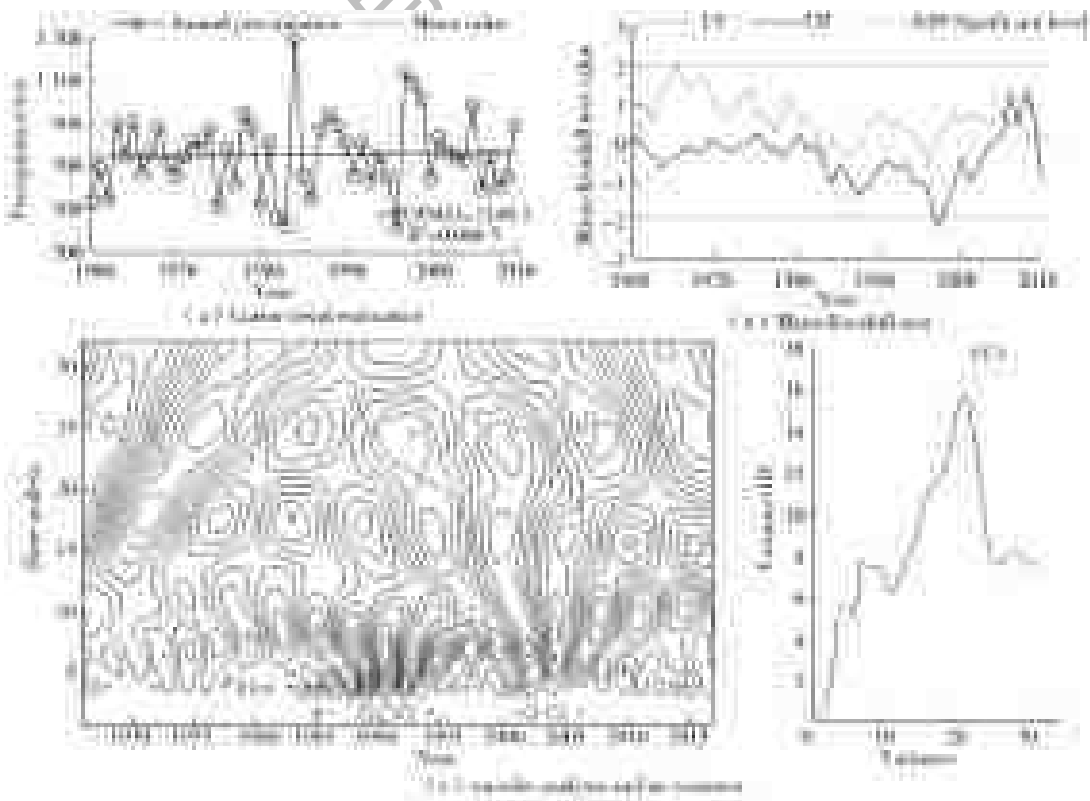

Fig. 3 Time series analysis of annual precipitation in the Dawen River basin

The results of Fig. 3(a) reveal that the overall increase of annual mean precipitation in the Dawen River basin was not significant ($p>0.01$) during the 52-year study period, with an average increase rate of 9.541 mm/(10 a). The results of the Mann-Kendall mutation test (Fig. 3(b)) show that the UF and UB curves intersected in 1989, 2011, and 2015, and all three of these intersection points are within the 95% confidence interval, indicating that the precipitation mutation points are 1989, 2011, and 2015.

The precipitation wavelet analysis and variance diagram of the Dawen River basin from 1966 to 2017 is shown in Fig. 3(c). The wavelet coefficient value represents the change between dry and wet. If the wavelet coefficient is greater than zero, this indicates that there is more precipitation and the study area is in the wet season; conversely, the study area is in the dry season. There are three dry-abundant alternating oscillations in precipitation on a 15-30 year time scale and four oscillations on a 12-25 year time scale. It can also be seen that the cyclical changes of these two scales during the overall time period were relatively stable and exhibited global characteristics. At a 3-8 year time scale, however, due to its short length, the cyclical changes are relatively insignificant. According to the wavelet variance diagram, the peak value of the wavelet variance was highest when the time scale is 28 years, indicating that the signal vibration is strongest when the scale is 28 years, which is the first main period.

3.2 Comparative analysis of spatial variation of meteorological elements

We used the inverse distance weight interpolation module of ArcGIS to analyze the spatial changes of maximum temperature, minimum temperature and precipitation between historical (1976-2017) and future (2026-2100) in Dawenhe River basin, and the results were shown in Fig. 4(a)-4(l). As shown in Fig. 4(a)-4(h), the maximum and minimum temperatures in the future will rise radially in the center of the north central region, and the spatial distribution will be roughly the same in different scenarios. The future precipitation is the highest in the north central region, and decreases radially to the surrounding. As the former two, there is almost no change in the spatial distribution of rainfall under different scenarios.

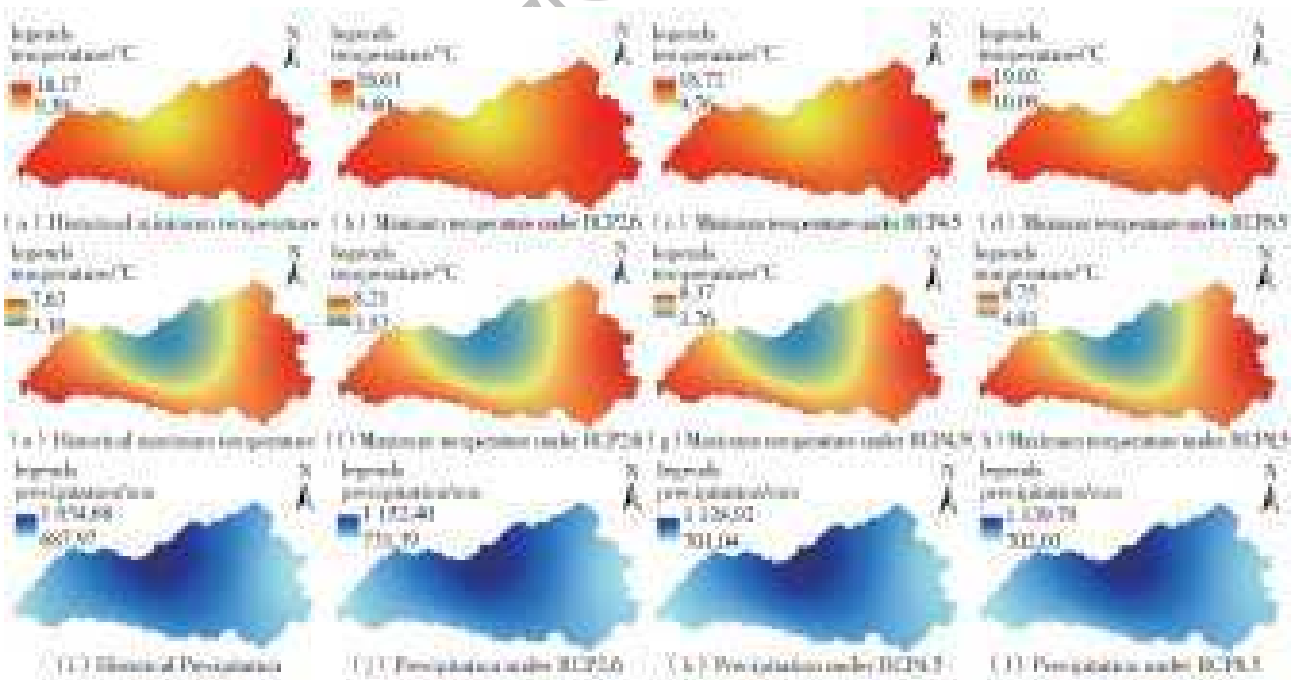

Fig. 4 Comparative analysis of spatial variation of meteorological element in the Dawen River basin

3.3 Comparative analysis of temporal variation of meteorological elements in the future

To better assess climate change, the baseline period (BP) is the 40 years from 1976 to 2015, while 1976-1995 and 1996-2015 are selected as the calibration and validation periods to construct the SDSM and to subsequently simulate the maximum

temperature, minimum temperature, and precipitation from 2026 to 2100 under the RCP2.6 (high global emission), RCP4.5 (moderate global emission), and RCP8.5 (low global emission) scenarios. To clearly analyze the changes in different periods, the simulation period was divided into the early phase (EP, 2026-2050), middle phase (MP, 2051-2075), and latter phase (LP, 2076-2100)[35].

3.3.1 Projected monthly maximum temperatures

Fig. 5 (a)-5(c) shows the variation of monthly maximum temperature under different scenarios and period. For the RCP2.6 scenario, during the EP, the average monthly maximum temperature increased by 0.29 ℃. June, October, and November are the largest increase, compared with the baseline period, the increase is 0.87 ℃, 0.81 ℃, and 1.20 ℃, respectively. During the MP, the average monthly maximum temperature increased by 0.48 ℃. Same as MP, June, October, and November are the months with the largest increase, the increases are 1.00 ℃, 0.93 ℃, and 1.15 ℃, respectively. During the LP, the average monthly maximum temperature rise is 0.49 ℃. June, October, and November are the months with the highest increase which is the same as that in the EP and MP, and the increases are 0.93 ℃, 1.01 ℃, and 1.51 ℃, respectively.

For the RCP4.5 scenario, the temperature of each period shows an upward trend. During the EP, the average monthly maximum temperature increased by 0.28 ℃, and the largest increase is June, October, and November, the increase is 0.85 ℃, 0.74 ℃, and 1.27 ℃, respectively. During the MP, the average monthly maximum temperature increased by 0.54 ℃, June, October, and November are the largest increase, with the increase of 1.00 ℃, 1.15 ℃, and 1.26 ℃, respectively. During the LP, the average monthly maximum temperature rise is 0.69 ℃. June, October, and November are the months with the largest increase, with an increase of 1.12 ℃, 1.36 ℃, and 1.73 ℃, respectively.

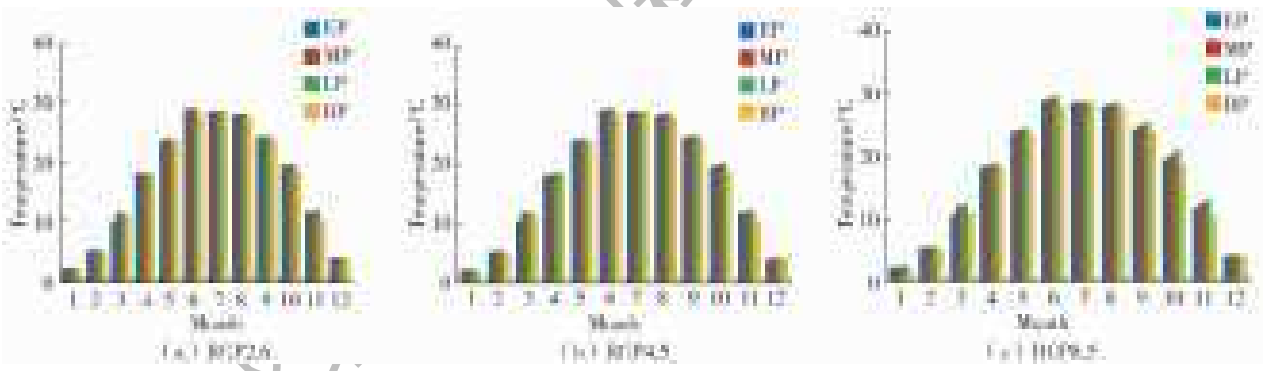

Fig. 5 Monthly mean annual maximum temperature for different scenarios

For the RCP8.5 scenario, as in the previous two scenarios, the trend is upward in all period. During the EP, the average monthly maximum temperature increased by 0.36 ℃, and the maximum temperature increase in June, October, and November, and the rise is 0.81 ℃, 0.84 ℃, and 1.20 ℃, respectively. During the MP, the average monthly maximum temperature increased by 0.75 ℃, which is the same as EP. June, October, and November are the months with the maximum temperature increase. Compared with the base period, the increases are 1.15 ℃, 1.42 ℃, and 1.89 ℃, respectively. During the LP, the average monthly maximum temperature increased by 1.11 ℃. Compared with the baseline period, June, October, and November are the months with the maximum temperature increase, and the increases are 1.43 ℃, 2.33 ℃, and 2.68 ℃, respectively.

Fig. 6 presents the average annual maximum temperatures for the RCP2.6, RCP4.5, and RCP8.5 scenarios. This figure shows that the annual maximum temperatures under the RCP4.5 and RCP8.5 scenarios are projected to increase over time, while the growth trend under the RCP2.6 scenario tends to be flat. Specifically, the RCP4.5 and RCP8.5 scenarios indicate that there may be increases in mean maximum temperature by 0.06 ℃/(10 a) and 0.15 ℃/(10 a), respectively.

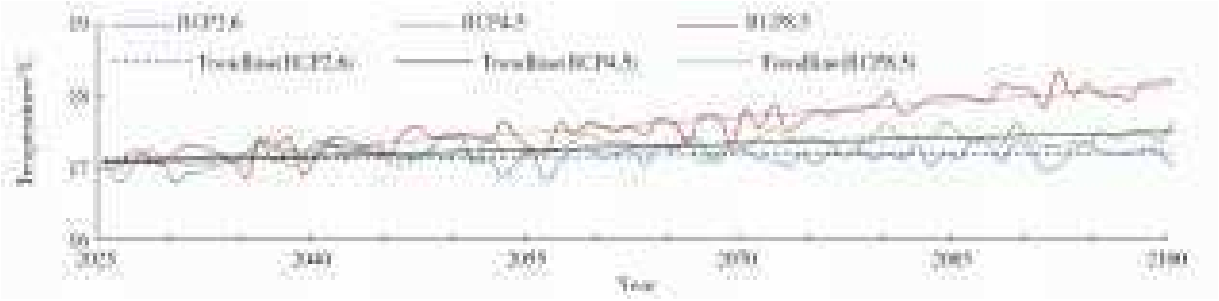

Fig. 6 Trends of average annual maximum temperature for different scenarios

In the different periods, the three scenarios forecast different changes. During the EP, the change curves of the three scenarios cross multiple times, the monthly maximum temperature in the basin fluctuates greatly, the average annual maximum temperatures do not differ significantly, and the growth trends are basically the same. Compared with the baseline period, the RCP2.6, RCP4.5, and RCP8.5 scenarios predict respective increases of 0.49 ℃, 0.46 ℃, and 0.58 ℃, with corresponding fluctuation ranges of 16.91–17.43 ℃, 16.80–17.42 ℃, and 16.89–17.58 ℃. During the MP, the average annual maximum temperature gap between the three scenarios becomes larger and the growth trends accelerate. The change trend of the RCP8.5 scenario is greater than that of the RCP4.5 or RCP2.6. Compared with the baseline period, the RCP2.6, RCP4.5, and RCP8.5 scenarios predict increases of 0.47 ℃, 0.64 ℃, and 0.87 ℃, respectively, with corresponding fluctuation ranges of 16.89–17.41 ℃, 17.06–17.55 ℃, and 17.27–17.88 ℃. During the LP, the average annual maximum temperature gap between the three scenarios changes significantly, and the relative growth trends are RCP2.6<RCP4.5<RCP8.5. Compared with the baseline period, the RCP2.6, RCP4.5, and RCP8.5 project increases of 0.51 ℃, 0.74 ℃, and 1.32 ℃, respectively, with corresponding fluctuation ranges of 16.94–17.37 ℃, 17.15–17.66 ℃, and 17.74–18.35 ℃, respectively.

3.3.2 Projected monthly minimum temperatures

Fig. 7(a)-(c) shows the variation of monthly minimum temperature under different scenarios and period. For the RCP2.6 scenario, During the EP, the average monthly minimum temperature increased by 0.39 ℃. the monthly minimum temperature in June and November are the largest increase, with an increase of 0.93 ℃ and 0.91 ℃, respectively. During the MP, the average monthly minimum temperature increased by 0.53 ℃. Same as EP, June and November are the months with the largest increase, with an increase of 1.09 ℃ and 0.80 ℃, respectively. During the LP, the average monthly minimum temperature rise is 0.58 ℃. June and November are the months with the largest increase, which is the same as that in the EP and MP. Compared with the base period, the increases are 1.08 ℃ and 1.11 ℃, respectively.

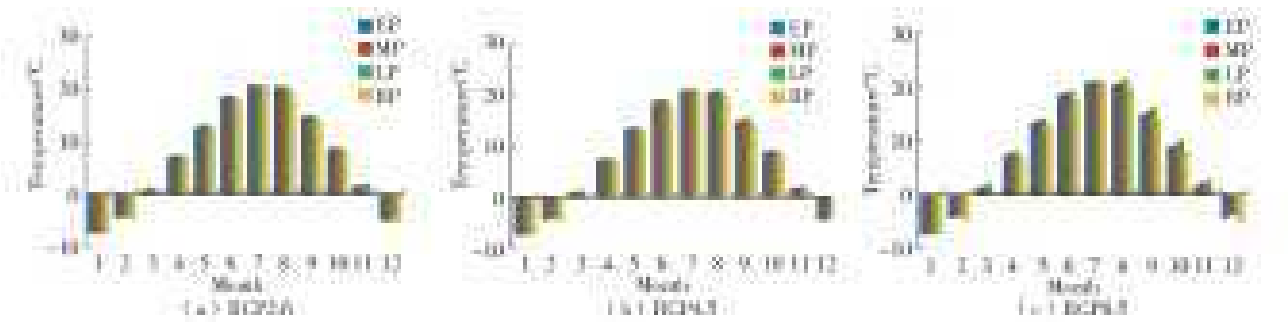

Fig. 7 Monthly mean annual minimum temperature for different scenarios

For the RCP4.5 scenario, During the EP, the average monthly minimum temperature increased by 0.50 ℃, the monthly minimum temperature in June, November, and December are the largest increase, with an increase of 1.02 ℃, 0.90 ℃ and 0.93 ℃, respectively. During the MP, the average

monthly minimum temperature increased by 0.54 ℃, and June, November and December are the largest increase, with the increase of 1.13 ℃, 0.94 ℃, and 0.80 ℃, respectively. During the LP, the average monthly minimum temperature rise is 0.69 ℃. Same as MP, June, November and December are the largest increase. Compared with the base period, the monthly minimum temperature increases by 1.34 ℃, 1.24 ℃, and 1.39 ℃, respectively.

For the RCP8.5 scenario, during the EP, the average monthly minimum temperature increased by 0.56 ℃, the monthly minimum temperature in June, November and December are the largest increase, with an increase of 0.95 ℃, 0.86 ℃, and 0.87 ℃, respectively. During the MP, the average monthly minimum temperature increased by 0.95 ℃, and June, November, and December are the largest increase, with the increase of 1.35 ℃, 1.34 ℃, and 1.58 ℃, respectively. During the LP, the average monthly minimum temperature rise is 1.30 ℃. Same as MP, June, November and December are the largest increase. Compared with the base period, the monthly minimum temperature increases by 1.68 ℃, 1.92 ℃, and 1.54 ℃, respectively.

Fig. 8 presents the average annual minimum temperature for the RCP2.6, RCP4.5, and RCP8.5 scenarios. The temperature increase predicted by the RCP8.5 scenario is the largest in the three periods, followed by the RCP4.5 scenario, while the temperature in the RCP2.6 scenario is basically unchanged. Specifically, the RCP4.5 and RCP8.5 scenarios indicate that there may be increases in mean maximum temperature by 0.06 ℃/(10 a) and 0.15 ℃/(10 a), respectively.

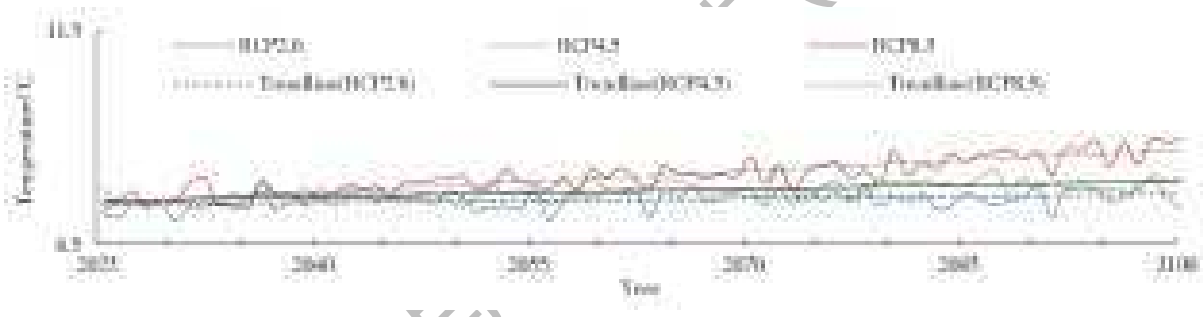

Fig. 8 Trends of average annual minimum temperature for different scenarios

During the EP, the average annual minimum temperatures projected by the three scenarios are not much different, and the growth trends are basically the same. The change trend of the RCP8.5 scenario, however, is slightly larger than that of the RCP4.5 or RCP2.6. Compared with the baseline period, the RCP2.6, RCP4.5, and RCP8.5 predict increases of 0.38 ℃, 0.45 ℃, and 0.62 ℃, respectively, with corresponding fluctuation ranges of 7.05-7.74 ℃, 7.36-7.92 ℃, and 7.32-8.06 ℃, respectively. During the MP, the gap between the average annual minimum temperatures of the three scenarios becomes larger and the growth trends accelerate. The change trend of the RCP8.5 scenario is still greater than that of the RCP4.5 or RCP2.6. Compared with the baseline period, the RCP2.6, RCP4.5, and RCP8.5 scenarios predict increases of 0.44 ℃, 0.66 ℃, and 0.96 ℃, respectively, with corresponding fluctuation ranges of 7.02-7.80 ℃, 7.50-8.34 ℃, and 7.72-8.54 ℃. During the LP, the gap between the average annual minimum temperature of the three scenarios becomes larger and the relative growth trend is RCP2.6＜RCP4.5＜RCP8.5. Compared with the baseline period, the RCP2.6, RCP4.5, and RCP8.5 project increases by 0.49 ℃, 0.79 ℃, and 1.42 ℃, respectively, with corresponding fluctuation ranges of 7.31-8.02 ℃, 7.61-8.25 ℃, and 7.93-8.96 ℃.

3.3.3 Projected monthly precipitation statistics

The best way to evaluate the characteristics of the change in precipitation pattern is by examining the monthly statistics. The monthly precipitation simulation results of the three scenarios are shown in Fig. 9(a)-(c). These results reveal the following.

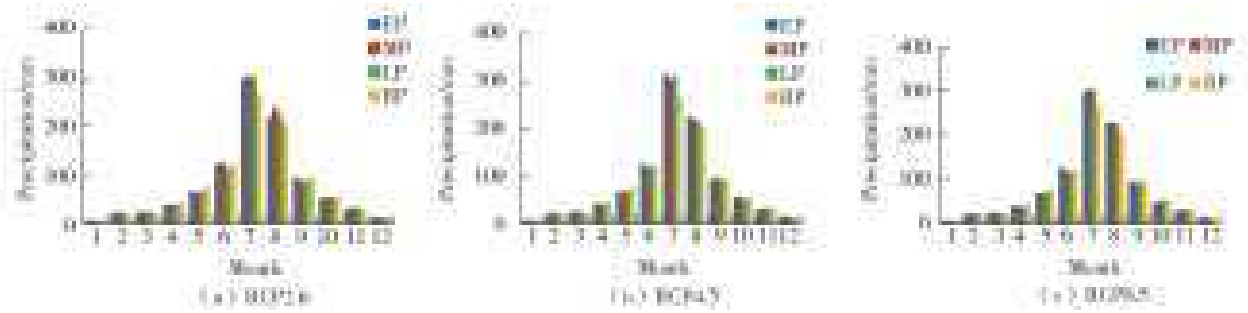

Fig. 9 Monthly mean annual precipitation for different scenarios

For the RCP2.6 scenario, the precipitation trend is increasing generally. And the increase is 2.79, 5.17, 2.92 mm for the EP, MP, and LP projections, respectively. The precipitation is projected to increase in February, March, July, August, and November, with the largest increases in July and August. Specifically, these increases are 31.09, 37.81, 36.27 mm in July and 14.73, 36.13, 21.62 mm in August for the EP, MP, and LP projections, respectively. For the RCP4.5 scenario, the precipitation trend is increasing generally. And the increase is 5.29, 4.09, 3.78 mm for the EP, MP, and LP projections, respectively. The predicted increases are also the largest in July and August, and slightly larger than RCP2.6. Specifically, these increases are 47.31, 37.95, 44.92 mm in July and 22.44, 16.54, 12.82 mm in August, respectively. For the RCP8.5 scenario, the precipitation trend is increasing generally. And the increase is 3.74, 3.81, 4.19 mm for the EP, MP, and LP projections, respectively. The future precipitation in February, March, July, August, and December exhibits an increasing trend. As with the previous two scenarios, the largest increases are projected to occur in July and August. Specifically, these increases are 28.82, 37.26, 34.20 mm in July and 14.73, 36.13, 21.62 mm in August, respectively.

Fig. 10 shows the average annual precipitation for the RCP2.6, RCP4.5, and RCP8.5 scenarios. There will be no obvious trend of precipitation in the next three scenarios. The projected precipitation will increase by 3.37, 0.53, −2.07 mm/(10 a) in RCP2.6, RCP4.5 and RCP8.5 scenarios, respectively.

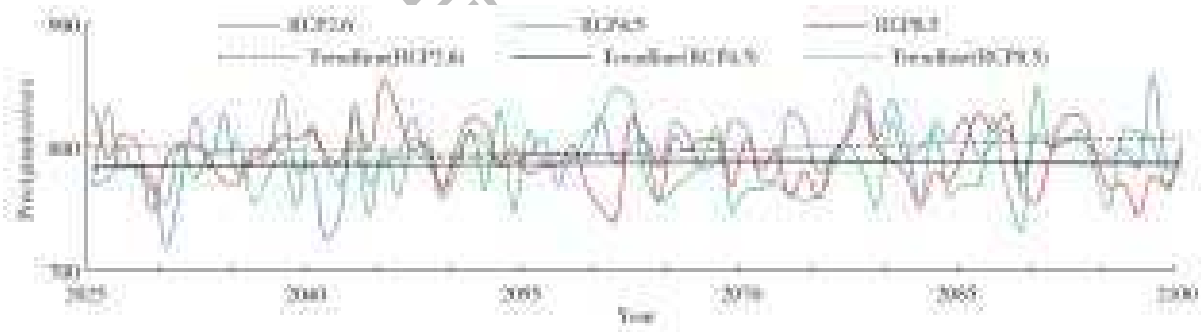

Fig. 10 Trends of average annual precipitation for different scenarios

During the EP, the trends in the RCP2.6, RCP4.5, and RCP8.5 scenarios are basically the same. The interannual precipitation varies greatly in all three scenarios. The average annual precipitation of the three scenarios are 785.81, 784.02, 798.02 mm, respectively. Compared with the baseline period, the RCP2.6, RCP4.5, and RCP8.5 predict increases of 53.84, 52.05, 66.05 mm, respectively, with corresponding fluctuation ranges of 719.55-841.15, 745.07-818.02, 747.83-855.43 mm. During the MP, the average annual precipitation of the RCP 2.6, RCP4.5, and RCP8.5 scenarios are 797.88, 787.22, 787.73 mm, respectively. Compared with the baseline period, the RCP2.6, RCP4.5, and RCP8.5 change by 65.92, 55.24, and 55.76 mm, respectively, with corresponding fluctuation ranges of 769.43-823.31, 846.87-747.20, 739.82-823.62 mm. During the LP, the differences in average annual precipitation among the three scenarios are small and basically the same. Compared with the baseline period, the RCP2.6, RCP4.5, and RCP8.5 increase by 72.03, 58.07, 58.20 mm,

respectively, with corresponding fluctuation ranges of 758.02-857.65, 750.64-848.22, 745.75-832.44 mm. Overall, there are no obvious precipitation trend changes during the EP, MP, and LP.

4 Discussion

4.1 Change features in the Dawen River basin

The temporal trend change features indicated that there was a warmer-wetter trend in the study area from 1966 to 2017. In fact, the increasing temperature trend of the Dawen River basin is greater than the global 0.14 ℃/(10 a) rate and China's 0.22 ℃/(10 a) rate[36]. This indicated that the semi-humid areas of China are more affected by global warming. This conclusion coincides with that of Xu et al.[37] on climate change research in Inner Mongolia. Although the annual precipitation of the Dawen River basin did not increase significantly, it fluctuated sharply after 1989, which is closely associated with the rapid urbanization of this region. According to the relevant data, over the past three decades, Chinese cities have experienced unprecedented growth, and the resulting urbanization process has exerted a significant impact on the hydrological cycle at the local and regional scales[38].

Spatially, elevation is closely related to changes in precipitation and temperature in the Dawen River basin. The rain gradient in complex terrain is usually not linearly related to elevation[39]. In terms of the spatial distribution of the climate in the Dawen River basin, however, precipitation is not completely independent of elevation, which may be related to monsoon activities, although specific conclusions still require scientific appraisal.

4.2 Characteristics of future changes in the Dawen River basin for different scenarios

The future maximum and minimum temperatures in the Dawen River basin were projected to increase with time in the RCP2.6, RCP4.5, and RCP8.5 scenarios. The predictions of global surface temperature from 2018 to 2100[40], as well as those of the Tibetan Plateau and most of northern China from 2011 to 2035, under the RCP4.5 scenario[41] displayed the same increase. This indicated that the continuous emission of greenhouse gases associated with global warming will progressively impact the temperatures of the Dawen River basin more seriously in the future. The relative predicted increases of annual and monthly average maximum temperature and minimum temperature in the Dawen River basin were expressed as RCP8.5 > RCP4.5 > RCP2.6, indicating a strong correlation between greenhouse gas emissions and temperature in the Dawen River basin, i.e., the more greenhouse gas emissions, the greater the temperature rise.

For the RCP2.6, RCP4.5, and RCP8.5 scenarios, there was no systematic difference in the variation trend of annual precipitation in the Dawen River basin. The annual curves had multiple intersections, and the precipitation in the RCP8.5 scenario was not always greater than the precipitation in the RCP4.5 and RCP2.6, confirming that the impact of greenhouse gas emissions on precipitation in the Dawen River basin was likely to be nonlinear. Lv Yanming's prediction of rainfall in China also supported this relationship[42]. Under the comprehensive influence of the East Asian monsoon, complex terrain, large amounts of aerosol emissions, and greenhouse gas emissions, the simulation and prediction of precipitation in China remains a huge challenge[43-44]. Therefore, a simulation that provided a more accurate prediction of interannual future precipitation was still required. The precipitation of the Dawen River basin exhibited pronounced seasonal changes, and the summer precipitation in the future was projected to be significantly higher than other seasons[45-46], which may be related to anomalies of large-scale climate indices.

5 Conclusions

Based on daily maximum and minimum temperature and precipitation data from 6 meteorological stations from 1966 to 2017, we analyzed the temporal and spatial changes of history and future in the Dawen River basin. The conclusions are as follows:

(1) From 1966 to 2017, the temperatures in the Dawen River basin exhibited a significant increasing trend ($p<0.01$), with a trend rate of 0.032 3

mm/a. Abrupt changes of temperature occurred in 1994 and 1996, and the main oscillation period was 28 years. The annual precipitation in the Dawen River basin showed an upward trend ($p>0.01$), and the trend rate was 0.954 1 mm/a. The abrupt changed occurred in 1989, 2011, and 2015, the main oscillation period was 22 years.

(2) The spatial distribution of historical temperature shows a trend of decreasing to the surroundings with the central and northern part as the center; On the contrary, the spatial distribution of historical precipitation shows a trend of increasing to the surroundings centered on the central and northern part. In different scenarios, the spatial distribution of the projected maximum temperature, minimum temperature and precipitation will hardly change compared with history.

(3) In the Dawen River basin, the overall temperature and precipitation will increase in the future. Under the three scenarios of RCP2.6, RCP4.5, and RCP8.5, the monthly average maximum temperature will increase by 0.42 ℃, 0.50 ℃, 0.74 ℃, and the monthly average minimum temperature will increase by 0.47 ℃, 0.58 ℃, 0.94 ℃, and the monthly average precipitation will increase by 3.63, 4.39, 3.91 mm respectively. The months with the largest monthly maximum temperature increase are concentrated in June, October, and November; the minimum temperature were June and November; the precipitation increase was concentrated in July and August.

(4) The annual maximum and minimum temperature were projected to gradually increase as the time scale increases under RCP4.5 and RCP8.5 scenarios. The projected maximum temperature will increase by 0.01 ℃/(10 a), 0.06 ℃/(10 a), and 0.15 ℃/(10 a) in RCP2.6, RCP4.5 and RCP8.5 scenarios, respectively. The projected minimum temperature will increase by 0.03 ℃/(10 a), 0.06 ℃/(10 a), and 0.17 ℃/(10 a) in RCP2.6, RCP4.5, and RCP8.5 scenarios, respectively. The projected precipitation will increase by 3.37, 0.53, −2.07 mm/(10 a) in RCP2.6, RCP4.5 and RCP8.5 scenarios, respectively. The future annual mean precipitation trend was not predicted to change significantly, with no obvious increase or decrease trend. For all scenarios, however, the fluctuation range of future precipitation was relatively large, indicating a high degree of uncertainty.

The results are helpful to understand and predict the future climate change in Dawen River basin under the condition of climate warming, and provide guidance for agricultural production in the basin.

Acknowledgments

This work was supported by the National Natural Science Foundation of China (Grant No. 41471160). The authors would also like to thank the reviewers for their very valuable comments, which greatly improved the quality of this manuscript.

References:

[1] CAI M, MURTAZASHVILI I, MURTAZASHVILI J B, et al. Patience and climate change mitigation: Global evidence [J]. Environmental Research, 2020, 186: 109552. DOI: https://doi.org/10.1016/j.envres.2020.109552.

[2] HARPER S L, WRIGHT C, MASINA S, et al. Climate change, water, and human health research in the Arctic [J]. Water Security, 2020, 10: 100062. DOI: https://doi.org/10.1016/j.wasec.2020.100062.

[3] SCHIPPER E L F, TANNER T, DUBE O P, et al. The debate: Is global development adapting to climate change? [J]. World Development Perspectives, 2020, 18: 100205. DOI: https://doi.org/10.1016/j.wdp.2020.100205.

[4] LIVINGSTON J E, RUMMUKAINEN M. Taking science by surprise: The knowledge politics of the IPCC Special Report on 1.5 degrees[J]. Environmental Science & Policy, 2020, 112: 10-16. DOI: https://doi.org/10.1016/j.envsci.2020.05.020.

[5] DE U S, DUBE R K, PRAKASA RAO G S. Extreme weather events over India in the last 100 years[J]. J Ind Geophys Union, 2005, 9.

[6] MIN S K, ZHANG X, ZWIERS F W, et al. Human contribution to more-intense precipitation extremes [J]. Nature, 2011, 378-381. DOI: 10.1038/nature09763.

[7] SHI J, CUI L, WANG J, et al. Changes in the temperature and precipitation extremes in China during 1961-2015[J]. Quaternary International, 2019, 527: 64-78. DOI: https://doi.org/10.1016/j.quaint.2018.08.008.

[8] TONG S, LI X, ZHANG J, et al. Spatial and temporal

variability in extreme temperature and precipitation events in Inner Mongolia (China) during 1960-2017 [J]. Science of The Total Environment, 2019, 649: 75-89. DOI: https://doi.org/10.1016/j.scitotenv.2018.08.262.

[9] DU X, SHRESTHA N K, WANG J. Assessing climate change impacts on stream temperature in the Athabasca River basin using SWAT equilibrium temperature model and its potential impacts on stream ecosystem[J]. Science of The Total Environment, 2019, 650: 1872-1881. DOI: https://doi.org/10.1016/j.scitotenv.2018.09.344.

[10] KUNDZEWICZ Z W, KRYSANOVA V, BENESTAD R E, et al. Uncertainty in climate change impacts on water resources[J]. Environmental Science & Policy, 2018, 79: 1-8. DOI: https://doi.org/10.1016/j.envsci.2017.10.008.

[11] YANG X, HE R, YE J, et al. Integrating an hourly weather generator with an hourly rainfall SWAT model for climate change impact assessment in the Ru River basin, China[J]. Atmospheric Research, 2020, 244: 105062. DOI: https://doi.org/10.1016/j.atmosres.2020.105062.

[12] NGUYEN G T H, SHIMADERA H, URANISHI K, et al. Numerical assessment of $PM_{2.5}$ and O_3 air quality in continental southeast Asia: Impacts of future projected anthropogenic emission change and its impacts in combination with potential future climate change impacts[J]. Atmospheric Environment, 2020, 226: 117398. DOI: https://doi.org/10.1016/j.atmosenv.2020.117398.

[13] LIU W, XU J, XIE X, et al. A new integrated framework to estimate the climate change impacts of biomass utilization for biofuel in life cycle assessment [J]. Journal of Cleaner Production, 2020, 267: 122061. DOI: https://doi.org/10.1016/j.jclepro.2020.122061.

[14] ALEXANDER L, ALLEN S, BINDOFF N L. Climate change 2013: The physical science basis, in contribution of Working Group I (WGI) to the Fifth Assessment Report (AR5) of the Intergovernmental Panel on Climate Change (IPCC)[C], 2013: 1535.

[15] JAVAHERIAN M, EBRAHIMI H, AMINNEJAD B. Prediction of changes in climatic parameters using CanESM2 model based on Rcp scenarios (case study): Lar dam basin[J]. Ain Shams Engineering Journal, 2020. DOI: https://doi.org/10.1016/j.asej.2020.04.012.

[16] GULACHA M M, MULUNGU D M M. Generation of climate change scenarios for precipitation and temperature at local scales using SDSM in Wami-Ruvu River basin Tanzania[J]. Physics and Chemistry of the Earth, Parts A/B/C, 2017, 100: 62-72. DOI: https://doi.org/10.1016/j.pce.2016.10.003.

[17] WILBY R L, DAWSON C W, BARROW E M. Sdsm: A decision support tool for the assessment of regional climate change impacts[J]. Environmental Modelling & Software, 2002, 17(2): 145-157. DOI: https://doi.org/10.1016/S1364-8152(01)00060-3.

[18] PHOLKERN K, SARAPHIROM P, SRISUK K. Potential impact of climate change on groundwater resources in the Central Huai Luang basin, northeast Thailand[J]. Science of The Total Environment, 2018, 633: 1518-1535. DOI: https://doi.org/10.1016/j.scitotenv.2018.03.300.

[19] ZHU R, ZHENG H, CROKE B F W, et al. Quantifying climate contributions to changes in groundwater discharge for headwater catchments in a major Australian basin[J]. Science of The Total Environment, 2020, 729: 138910. DOI: https://doi.org/10.1016/j.scitotenv.2020.138910.

[20] ZHAO Z, WANG H, YU C, et al. Changes in spatiotemporal drought characteristics over northeast China from 1960 to 2018 based on the modified nested copula model[J]. Science of The Total Environment, 2020, 739: 140328. DOI: https://doi.org/10.1016/j.scitotenv.2020.140328.

[21] ZHOU Z, SHI H, FU Q, et al. Assessing spatiotemporal characteristics of drought and its effects on climate-induced yield of maize in northeast China[J]. Journal of Hydrology, 2020, 588: 125097. DOI: https://doi.org/10.1016/j.jhydrol.2020.125097.

[22] HU Q, PAN F, PAN X, et al. Spatial analysis of climate change in Inner Mongolia during 1961-2012, China[J]. Applied Geography, 2015, 60: 254-260. DOI: https://doi.org/10.1016/j.apgeog.2014.10.009.

[23] FAN K, ZHANG Q, SINGH V P, et al. Spatiotemporal impact of soil moisture on air temperature across the Tibet Plateau[J]. Science of The Total Environment, 2019, 649: 1338-1348. DOI: https://doi.org/10.1016/j.scitotenv.2018.08.399.

[24] MUMTAZ U, ALI Y, PETRILLO A. A linear regression approach to evaluate the green supply chain management impact on industrial organizational performance[J]. Science of The Total Environment, 2018, 624: 162-169. DOI: https://doi.org/10.1016/j.scitotenv.2017.12.089.

[25] LIVADA I, SYNNEFA A, HADDAD S, et al. Time series analysis of ambient air-temperature during the period 1970-2016 over Sydney, Australia[J]. Science of The Total Environment, 2019, 648: 1627-1638. DOI: https://doi.org/10.1016/j.scitotenv.2018.08.144.

[26] WU C, JI C, SHI B, et al. The impact of climate change

and human activities on streamflow and sediment load in the Pearl River basin[J]. International Journal of Sediment Research, 2019, 34(4): 307-321. DOI: https://doi.org/10.1016/j.ijsrc.2019.01.002.

[27] MUMO L, YU J, AYUGI B. Evaluation of spatiotemporal variability of rainfall over Kenya from 1979 to 2017[J]. Journal of Atmospheric and Solar-Terrestrial Physics, 2019, 194: 105097. DOI: https://doi.org/10.1016/j.jastp.2019.105097.

[28] SAMADI S, EHTERAMIAN K, SARRAF B S. SDSM ability in simulate predictors for climate detecting over Khorasan province[J]. Procedia-Social and Behavioral Sciences, 2011, 19: 741-749. DOI: https://doi.org/10.1016/j.sbspro.2011.05.193.

[29] GÜÇLÜ Y S. Improved visualization for trend analysis by comparing with classical Mann-Kendall test and ITA[J]. Journal of Hydrology, 2020, 584: 124674. DOI: https://doi.org/10.1016/j.jhydrol.2020.124674.

[30] MORLET D, COUDERC J P, TOUBOUL P, et al. Wavelet analysis of high-resolution ECGs in post-infarction patients: role of the basic wavelet and of the analyzed lead[J]. International Journal of Bio-Medical Computing, 1995, 39(3): 311-325. DOI: https://doi.org/10.1016/0020-7101(95)01113-S.

[31] MARUYAMA F, KAI K, MORIMOTO H. Wavelet-based multifractal analysis on a time series of solar activity and PDO climate index[J]. Advances in Space Research, 2017, 60(6): 1363-1372. DOI: https://doi.org/10.1016/j.asr.2017.06.004.

[32] XU J. Wavelet regression: An approach for undertaking multi-time scale analyses of hydro-climate relationships[J]. MethodsX, 2018, 5: 561-568. DOI: https://doi.org/10.1016/j.mex.2018.05.005.

[33] REZAEI A, GURDAK J J. Large-scale climate variability controls on climate, vegetation coverage, lake and groundwater storage in the Lake Urmia watershed using SSA and wavelet analysis[J]. Science of The Total Environment, 2020, 724: 138273. DOI: https://doi.org/10.1016/j.scitotenv.2020.138273.

[34] LEE E, KIM S. Wavelet analysis of soil moisture measurements for hillslope hydrological processes[J]. Journal of Hydrology, 2019, 575: 82-93. DOI: https://doi.org/10.1016/j.jhydrol.2019.05.023.

[35] PARK C-K, BYUN H-R, DEO R, et al. Drought prediction till 2100 under RCP 8.5 climate change scenarios for Korea[J]. Journal of Hydrology, 2015, 526: 221-230. DOI: https://doi.org/10.1016/j.jhydrol.2014.10.043.

[36] REN G, GUO j, XU M, et al. Basic characteristics of surface climate change in China in recent 50 years(in Chinese)[J]. Acta Meteorologica Sinica, 2005, (6): 942-956.

[37] XU L, YU G, ZHANG W, et al. Change features of time-series climate variables from 1962 to 2016 in Inner Mongolia, China[J]. Journal of Arid Land, 2020, 12(1): 58-72.

[38] GU X, ZHANG Q, LI J, et al. Impact of urbanization on nonstationarity of annual and seasonal precipitation extremes in China[J]. Journal of Hydrology, 2019, 575: 638-655. DOI: https://doi.org/10.1016/j.jhydrol.2019.05.070.

[39] SINGH P, KUMAR N. Impact assessment of climate change on the hydrological response of a snow and glacier melt runoff dominated Himalayan River[J]. Journal of Hydrology, 1997, 193(1): 316-350. DOI: https://doi.org/10.1016/S0022-1694(96)03142-3.

[40] MOSS R H, EDMONDS J A, HIBBARD K A, et al. The next generation of scenarios for climate change research and assessment[J]. Nature, 2010, 463: 747-756.

[41] ZHI X F, WANG J, LIN C Z, et al. Study on BMA prediction method of temperature in CMIP5 multi model data[J]. Journal of the Meteorological Sciences, 2015, 35(4): 405-412.

[42] LV Y, GUO J, YIM S H-L, et al. Towards understanding multi-model precipitation predictions from CMIP5 based on China hourly merged precipitation analysis data[J]. Atmospheric Research, 2020, 231: 104671. DOI: https://doi.org/10.1016/j.atmosres.2019.104671.

[43] GUO J, LIU H, WANG F, et al. Three-dimensional structure of aerosol in China: A perspective from multi-satellite observations[J]. Atmospheric Research, 2016, 178-179: 580-589. DOI: https://doi.org/10.1016/j.atmosres.2016.05.010.

[44] GUO J P, ZHANG X Y, WU Y R, et al. Spatio-temporal variation trends of satellite: based aerosol optical depth in China during 1980-2008[J]. Atmospheric Environment, 2011, 45(37): 6802-6811. DOI: https://doi.org/10.1016/j.atmosenv.2011.03.068.

[45] ZHANG Q, LI J, SINGH V P, et al. Influence of ENSO on precipitation in the East River basin, south China[J]. Journal of Geophysical Research: Atmospheres, 2013, 118(5): 2207-2219. DOI: 10.1002/jgrd.50279.

[46] WANG X, WANG B, XU X. Effects of large-scale climate anomalies on trends in seasonal precipitation over the Loess Plateau of China from 1961 to 2016[J]. Ecological Indicators, 2019, 107: 105643. DOI: https://doi.org/10.1016/j.ecolind.2019.105643.